Research Square

Preprints are preliminary reports that have not undergone peer review.
They should not be considered conclusive, used to inform clinical practice,
or referenced by the media as validated information.

ASC-directed nanobodies reduce inflammasome signaling and improve outcome after experimental ischemic stroke

Milena Strootmann
University Hospital Würzburg
Salie Maasewerd
University of Bonn
Lukas Rossnagel
University of Bonn
Florian I. Schmidt
University of Bonn
Bernardo S. Franklin
University of Bonn
Maximilian Bellut
bellut_m@ukw.de

University Hospital Würzburg

Research Article

Keywords: Ischemic stroke, Inflammasome, ASC, Nanobody, Single-domain antibody, NLRP3, AIM2, Pyroptosis, Neuroinflammation, Middle cerebral artery occlusion

Posted Date: November 19th, 2026

DOI: https://doi.org/10.21203/rs.3.rs-11636317/v1

License: This work is licensed under a Creative Commons Attribution 4.0 International License.
Read Full License

Additional Declarations: No competing interests reported.

ASC-directed nanobodies reduce inflammasome signaling and improve outcome after experimental ischemic stroke

Milena Strootmann[1], Salie Maasewerd[2], Lukas Rossnagel[2], Florian I. Schmidt[2], Bernardo S. Franklin[2,*], Maximilian Bellut[1,3,*]

[1]*University Hospital Würzburg, Department of Neurology, Würzburg, Germany*

[2]*Institute of Innate Immunity, Medical Faculty, University of Bonn, Bonn, Germany*

[3]*corresponding author: bellut_m@ukw.de*

**contributed equally*

Abstract

Background: Inflammasome activation contributes to ischemic brain injury, but therapeutic efforts have focused almost exclusively on individual upstream sensors such as NLR family pyrin domain-containing 3 (NLRP3). Because the inflammatory landscape shifts as persistent vessel occlusion gives way to reperfusion, inhibiting one sensor may protect incompletely. Methods: We targeted apoptosis-associated speck-like protein containing a caspase recruitment domain (ASC), the adaptor shared by multiple canonical inflammasomes, using a camelid-derived single-domain antibody (nanobody), VHH(mASC), in two complementary mouse models of ischemic stroke: permanent middle cerebral artery occlusion without reperfusion, and transient occlusion followed by reperfusion. Results: Applied before ischemia, during persistent occlusion, or immediately after reperfusion, VHH(mASC) reduced infarct volume by up to 61% and improved neurological function in every paradigm. Fluorescently labeled nanobody was enriched within ischemic brain tissue, and treatment lowered cerebral ASC abundance. ASC-positive neutrophils predominated during occlusion, whereas ASC-positive neurons and microglia were most abundant at the

later time point after reperfusion. Treatment attenuated signaling associated with NLRP3 and with absent in melanoma 2 (AIM2), and reduced caspase-1 activation, interleukin-1β maturation and gasdermin D (GSDMD) cleavage. Conclusions: ASC-directed nanobodies limit inflammasome signaling and improve outcome in acute ischemic stroke whether or not the occluded vessel is reopened, establishing adaptor-level inhibition as a strategy distinct from targeting individual sensors.

Keywords

Ischemic stroke; Inflammasome; ASC; Nanobody; Single-domain antibody; NLRP3; AIM2; Pyroptosis; Neuroinflammation; Middle cerebral artery occlusion

Background

Recanalization has fundamentally transformed the treatment of acute ischemic stroke (AIS)[1]. Nevertheless, even rapid restoration of cerebral blood flow does not necessarily terminate tissue injury. While neurons within the ischemic core are lost rapidly, potentially viable cells in the surrounding penumbra remain exposed to a dynamically evolving combination of metabolic failure, sterile inflammation, vascular dysfunction, and – following successful recanalization – reperfusion-associated stress [2,3]. Consequently, cerebral ischemia is not a single injurious event that ends when an occluded artery is reopened. Sterile inflammation is initiated within minutes of persistent arterial occlusion, driven by metabolic failure, danger-associated molecular patterns, endothelial activation, and the rapid recruitment and activation of innate immune cells, including neutrophils [4]. Restored blood flow does not initiate inflammation de novo but fundamentally reshapes an already heterogeneous inflammatory response by introducing oxidative stress,

restoring immune cell access, promoting blood–brain barrier disruption, and facilitating additional leukocyte infiltration and secondary tissue injury [5,6]. These two conditions — tissue under ongoing occlusion and tissue after restored perfusion — therefore represent qualitatively distinct inflammatory states rather than successive stages of the same process.

Inflammasomes have emerged as important molecular interfaces between ischemic cellular stress and the execution of inflammatory injury [7]. These cytosolic multiprotein complexes detect pathogen- or damage-associated signals and promote the activation of inflammatory caspases [8]. In canonical inflammasome signaling, activated caspase-1 cleaves the precursors of interleukin (IL)-1β and IL-18 and induces gasdermin D (GSDMD)-dependent membrane permeabilization and pyroptotic cell death [9]. The adaptor protein apoptosis-associated speck-like protein containing a caspase recruitment domain (ASC) connects several inflammasome sensors to procaspase-1 and oligomerizes into a supramolecular structure termed the ASC speck [10]. Thus, ASC speck formation not only serves as an intracellular platform that concentrates caspase-1 activation but also enables the persistence and extracellular propagation of inflammasome signaling after pyroptotic cell death [11,12].

Among the different inflammasomes, NLR family pyrin domain-containing 3 (NLRP3) has been studied most extensively in cerebral ischemia [13]. NLRP3 can respond to multiple consequences of acute energy failure, including potassium efflux, extracellular ATP, mitochondrial dysfunction, reactive oxygen species, lysosomal injury, and ionic disequilibrium [14]. Genetic or pharmacological interference with this pathway has repeatedly reduced inflammatory injury and improved neurological outcome in experimental stroke models. Selective pharmacological inhibition with MCC950 has established NLRP3 as a therapeutically accessible component of ischemic neuroinflammation [5,15–17]. Neuronal NLRP3 activation has also been shown to contribute directly to acute ischemic injury, indicating that inflammasome signaling is not confined to infiltrating or resident immune cells [13].

Despite the compelling evidence supporting NLRP3, the remarkable diversity of danger-associated molecular patterns generated during cerebral ischemia makes it unlikely that inflammatory signaling is mediated exclusively by a single inflammasome sensor [14]. To date, experimental evidence implicates additional ASC-dependent inflammasomes, including NLRP1 (NLR family pyrin domain-containing 1), AIM2 (absent in melanoma 2), and NLRC4 (NLR family CARD domain-containing protein 4), in ischemic brain injury. NLRP1 has been linked to neuronal injury, NLRC4 to microglial inflammatory responses, and AIM2 to sensing cytosolic double-stranded DNA released from damaged cells [18–20].

These observations identify ASC as an attractive therapeutic target. As the central adaptor protein required for the assembly of multiple canonical inflammasomes, ASC integrates inflammatory signaling downstream of diverse danger sensors [11]. Consequently, targeting ASC offers the opportunity to simultaneously attenuate several inflammasome pathways rather than inhibiting a single upstream receptor. However, because ASC also contributes to physiological inflammasome responses required for host defense and tissue homeostasis, broad intracellular inhibition may come at the expense of host protection [7]. An ideal therapeutic strategy would therefore selectively interfere with pathological ASC signaling while preserving inflammasome activity in unaffected cells.

Recently developed ASC-specific single-domain nanobodies may fulfill these requirements [21]. Owing to their inability to efficiently penetrate intact plasma membranes, extracellularly administered nanobodies largely fail to enter healthy or merely primed cells. Instead, they become accessible to intracellular ASC specks following pyroptotic membrane permeabilization and subsequently neutralize intracellular as well as extracellular ASC aggregates [21]. By dismantling these highly inflammatory post-pyroptotic ASC specks – which can persist extracellularly, propagate inflammasome activation in neighboring cells, and amplify inflammation in a prion-like manner – ASC nanobodies interrupt pathological inflammasome propagation [12,21]. Proof-of-concept

studies in experimental arthritis have demonstrated that this approach effectively reduces inflammation in vivo [21].

This mechanism may be particularly attractive in AIS, where pyroptotic cell death is a prominent feature of lesion evolution and is expected to promote the release of extracellular ASC specks [12,22]. As the inflammatory landscape changes substantially during the transition from persistent vessel occlusion to reperfusion, the relative contribution of individual ASC-dependent inflammasome sensors may likewise differ between these two conditions. Targeting their common adaptor may therefore provide coverage in both, whereas selective inhibition of a single sensor may not.

Because a single experimental paradigm cannot reproduce both of these inflammatory states, we deliberately used two complementary models rather than one. Permanent middle cerebral artery occlusion (pMCAO) reproduces ongoing ischemia in the absence of reperfusion, whereas transient occlusion followed by reperfusion (tMCAO) reproduces the situation after successful recanalization. Using both paradigms, we investigated whether ASC nanobody treatment limits inflammasome propagation and improves outcome during persistent vessel occlusion as well as after ischemia–reperfusion.

Methods

Experimental model and study design

The present study was designed to investigate whether pharmacological inhibition of the inflammasome adaptor protein ASC attenuates ischemic brain injury during both persistent vessel occlusion and ischemia–reperfusion. Male C57BL/6N mice were subjected to either permanent middle cerebral artery occlusion (pMCAO) for 4 h or transient middle cerebral artery occlusion (tMCAO) consisting of 60 min arterial occlusion followed by 23 h reperfusion. The two paradigms were chosen deliberately and address different clinical situations rather than serving as technical

replicates of one another. In pMCAO the artery remains occluded throughout, reproducing the situation of a patient in whom the vessel is not reopened, and — within the first hours after onset — the phase that every stroke patient passes through before recanalization. In tMCAO the occluding filament is withdrawn after 60 min so that blood flow is restored, reproducing successful recanalization by thrombolysis or thrombectomy and adding reperfusion-associated injury. Because these inflammatory environments differ, a treatment effective in only one of them would be of limited clinical value; VHH(mASC) was therefore tested in both. The observation periods follow from the models themselves. Permanent occlusion was terminated at 4 h; beyond this point continued occlusion is associated with an unacceptably high proportion of animals dying before the end of the observation period. The reperfusion paradigm is assessed 24 h after stroke onset (60 min occlusion plus 23 h reperfusion), the established endpoint for this model. A permanent-occlusion condition matched to that observation time can therefore not be generated. Each paradigm is analyzed against its own concurrent control group rather than against the other. Successful vessel occlusion and, in the transient paradigm, subsequent reperfusion were verified in every animal by intraoperative measurement of cerebral blood flow; animals not meeting the predefined flow criteria were not included; in the present cohorts, all animals met these criteria.

To assess prophylactic efficacy, mice undergoing pMCAO received an ASC-specific single-domain nanobody (VHH(mASC)) immediately before induction of ischemia. To evaluate therapeutic efficacy, additional cohorts received VHH(mASC) either 60 min after induction of permanent ischemia or immediately after reperfusion following 60 min tMCAO. Control animals received the same dose of an influenza A-specific nanobody inert in stroke (VHH(Inf. A)).

Primary outcome measures comprised infarct volume and neurological function. Secondary analyses investigated cerebral ASC abundance, cellular localization of ASC, cerebral exposure to fluorescently labeled VHH(mASC), assessed in a separate 4 h pMCAO cohort receiving a reduced dose of labeled nanobody (see below), inflammasome activation, and downstream inflammatory

and pyroptotic signaling by immunofluorescence, conventional western blotting, Wes automated capillary western immunoassay and NLRP3 immunoprecipitation.

Animals were randomized to treatment groups by an investigator not involved in surgery or outcome assessment. All surgical procedures, histological analyses, protein analyses and data evaluation were performed fully blinded to treatment allocation. One animal in the VHH(Inf. A) control group of the pMCAO cohort and one animal in the VHH(Inf. A) control group of the tMCAO cohort died before the end of the observation period and could not be analyzed. No further animals were lost, no predefined exclusion criteria were met, and no animals were excluded from analysis.

Animals

Male C57BL/6N mice (12–16 weeks of age, body weight 22–26 g) were housed under specific pathogen-free conditions with ad libitum access to food and water under a 12 h light/dark cycle. All experimental procedures were approved by the Government of Lower Franconia (Regierung von Unterfranken; approval number 2-2118) and performed in accordance with institutional guidelines and the ARRIVE recommendations.

Experimental cerebral ischemia

Permanent and transient focal cerebral ischemia were induced using the intraluminal filament model as previously described [23]. In this model a silicone-coated filament is advanced through the internal carotid artery until it occludes the origin of the middle cerebral artery. The artery itself is not injured, so withdrawal of the filament restores blood flow. The surgical procedure is thus identical in both paradigms, and the only difference between them is whether the filament is left in place (permanent ischemia) or withdrawn after a prespecified time (transient ischemia). For permanent ischemia, the middle cerebral artery remained occluded for 4 h before tissue collection. For transient ischemia, cerebral blood flow was restored after 60 min by careful withdrawal of the intraluminal filament, followed by 23 h reperfusion. Sham-operated animals underwent identical anesthesia, surgical preparation and vessel exposure, but the filament was not

advanced into the middle cerebral artery; they were operated in parallel with each paradigm (n = 3 per paradigm). Anesthesia, perioperative monitoring, body temperature control, surgical preparation and postoperative care were identical to the procedures described in our previous work [5].

Nanobody treatment

The murine ASC-specific single-domain nanobody VHH(mASC) and the biologically inert influenza A-specific control nanobody (VHH(Inf. A)) were provided by the group of Florian Schmidt at the Institute of Innate Immunity, Bonn, Germany. Nanobodies were administered intraperitoneally at a dose of 5 µg/g body weight – the dose established by dose titration for systemic VHH(mASC) administration in vivo [21] – in a total injection volume of 100 µl PBS. Three treatment paradigms were investigated. (i) Prophylactic treatment: Animals undergoing 4 h pMCAO received VHH(mASC) immediately before induction of cerebral ischemia (hereafter 4 h pMCAO). Control animals received an equivalent dose of VHH(Inf. A). (ii) Therapeutic treatment during persistent vessel occlusion: Animals undergoing 4 h pMCAO received VHH(mASC) 60 min after induction of ischemia and remained under vessel occlusion for an additional 3 h (hereafter 1+3 h pMCAO). Control animals received an equivalent dose of VHH(Inf. A). (iii) Therapeutic treatment following reperfusion: Animals subjected to 60 min tMCAO received VHH(mASC) immediately after filament withdrawal and initiation of reperfusion (hereafter 1+23 h tMCAO). Control animals received VHH(Inf. A) according to the identical treatment schedule.

To visualize whether systemically administered nanobody reaches the ischemic lesion, a separate cohort of mice subjected to 4 h pMCAO received Alexa Fluor™ 488-conjugated VHH(mASC) immediately before induction of ischemia at 0.5 µg/g body weight, corresponding to 10% of the therapeutic dose, in a total injection volume of 100 µl PBS. This reduced dose was chosen for visualization only and is not expected to meaningfully alter lesion development. Infarct volumes in this cohort were comparable to those of control animals. These animals were used exclusively for imaging and did not contribute to the outcome or biochemical analyses.

Neurological assessment

Neurological function was evaluated immediately before euthanasia using the composite neuroscore consisting of the inverted Bederson score and the grip test, applied exactly as described in our previous work [5,16]. Both subtests were scored from 0 to 5 points: the inverted Bederson score grades global neurological deficit, and the grip test grades motor function and coordination. The composite score ranged from 0 to 10 points, with 10 points indicating normal neurological function and 0 points indicating maximal neurological impairment. Scoring was performed by investigators blinded to treatment allocation.

Tissue collection and processing

Following neurological assessment, mice were deeply anesthetized and euthanized. Brains were rapidly removed and cut into three consecutive 2-mm-thick coronal sections using a murine brain matrix. The central coronal section, encompassing the MCA territory, was embedded in Tissue-Tek® O.C.T. Compound, snap-frozen, and cryosectioned into 10-µm coronal sections using a cryostat. Sections were mounted onto Superfrost Plus™ microscope slides and stored at -20°C until further histological processing. The anterior and posterior brain sections were immediately processed for biochemical analyses. Cerebral tissue from both hemispheres was dissected, snap-frozen in liquid nitrogen, and stored at -80°C until protein extraction.

Infarct volume determination

Infarct volume was determined by microtubule-associated protein 2 (MAP2) immunohistochemistry. Brain sections were immunostained for MAP2. Whole-slide images were acquired using an Epson Perfection V190 Scanner under identical acquisition settings for all animals. Infarct areas, defined as regions lacking MAP2 immunoreactivity, were quantified using Fiji (ImageJ, version 1.54p) by investigators blinded to treatment allocation. Infarct volume was calculated from serial 10-µm coronal sections sampled at regular intervals of 1 mm throughout the central 2-mm

coronal block encompassing the MCA territory (3 sections per animal). Volumes were corrected for cerebral edema using the indirect infarct volume method as previously described [24].

Immunofluorescence

Immunofluorescence was performed on 10-µm cryosections mounted on Superfrost Plus™ slides. Fluorescence images were acquired using an Axio Imager.M2 microscope equipped with an ApoTome.2 optical sectioning system, a Colibri 7 LED illumination system, and an Axiocam 506 mono camera (Carl Zeiss, Oberkochen, Germany). Images were acquired using identical microscope settings and processed identically for figure preparation. Detailed information on antibodies, chemicals and dilutions is provided in Additional file 1: Table S1 and Table S2.

To assess cerebral access of the nanobody, cryosections from mice that had received Alexa Fluor™ 488-conjugated VHH(mASC) at 10% of the therapeutic dose before 4 h pMCAO were mounted using DAPI-containing mounting medium and imaged directly, without additional immunostaining. Sections from n = 5 animals were imaged with consistent results. Nanobody-derived fluorescence was quantified from whole-hemisphere images acquired with identical settings: mean fluorescence intensity was measured in Fiji after background subtraction in the ipsilesional and in the contralateral hemisphere of the same section and is reported as the ipsilesional-to-contralateral ratio. Each animal thereby serves as its own internal reference, and the contralateral hemisphere provides a within-section control for autofluorescence and unspecific background. Because this cohort comprised a single treatment group, the ratio is reported for each animal individually and was not subjected to statistical testing.

Independently, Alexa Fluor™ 488-conjugated VHH(mASC) was used as a detection reagent on cryosections from mice treated with VHH(mASC) or VHH(Inf. A) at the therapeutic dose, to visualize nanobody-detectable ASC after treatment (n = 8 per group). Sections were fixed in ice-cold 100 % methanol, permeabilized and blocked as described below for ASC co-immunofluorescence, and were then incubated with Alexa Fluor™ 488-conjugated VHH(mASC) diluted 1:5000 in blocking

buffer for 2 h at room temperature; the nanobody was thus applied in the same way as a conventional primary antibody. Because the nanobody is directly fluorophore-conjugated, no secondary antibody incubation was required. Sections were subsequently washed, counterstained with DAPI and mounted using antifade mounting medium. An isotype control was processed in parallel at the same dilution to confirm staining specificity. Because the therapeutic nanobody and the detection reagent share the same epitope, a reduced signal may reflect reduced ASC abundance, epitope occupancy, or both; this readout is therefore interpreted alongside the ASC immunoblot described below. Nanobody-derived ASC signal was quantified as described above and is likewise reported as the ipsilesional-to-contralateral intensity ratio. Alexa Fluor™ 488 fluorescence was acquired in the corresponding detection channel and assigned a red lookup table for display, so that nanobody administered in vivo is distinguishable from the ex vivo nanobody staining displayed in green.

Cellular localization of ASC was assessed by co-immunofluorescence with NeuN, Iba1, or Ly6G. For ASC/Ly6G staining, cryosections were fixed with 100 % ice-cold methanol, permeabilized, blocked and incubated with primary antibodies against ASC and Ly6G, followed by species-specific fluorophore-conjugated secondary antibodies and DAPI counterstaining.

For ASC/Iba1 co-immunofluorescence, sections were fixed with 4% paraformaldehyde, permeabilized, blocked and incubated with rabbit anti-Iba1 followed by Alexa Fluor™ 488-conjugated $F(ab')_2$ goat anti-rabbit secondary antibody. After washing, sections were incubated with mouse anti-ASC followed by Alexa Fluor™ 647-conjugated $F(ab')_2$ goat anti-mouse secondary antibody. Sections were counterstained with DAPI and mounted using antifade mounting medium.

ASC/NeuN co-immunofluorescence was performed sequentially. Cryosections were fixed in ice-cold 100 % methanol, blocked and incubated with unconjugated goat anti-mouse Fab fragments before each incubation with a mouse-derived primary antibody. NeuN was detected using an Alexa Fluor™ 488-conjugated $F(ab')_2$ goat anti-mouse secondary antibody. After a second Fab-

fragment blocking step, ASC was detected using an Alexa Fluor™ 647-conjugated $F(ab')_2$ goat anti-mouse secondary antibody. Sections were counterstained with DAPI and mounted using antifade mounting medium. Quantification of ASC-positive cells was performed across the entire ipsilesional hemisphere rather than in a preselected region, and cell counts are expressed per 10 mm^2 for all three co-stainings. Representative images shown in the figures were selected for image quality and do not define the region used for quantification.

Preparation of protein lysates

For biochemical analyses, cortical and basal ganglia tissue was dissected from the anterior and posterior coronal brain sections as described above. Tissue was homogenized on ice in CelLytic™ MT Cell Lysis Reagent supplemented with Complete™ protease inhibitor and phosphatase inhibitor using disposable homogenization pestles. Homogenates were sonicated for 20 s, centrifuged at 13,000 x g for 30 min at 4°C, and supernatants were collected. Protein concentrations were determined using the bicinchoninic acid (BCA) assay before sample preparation for immunoblotting.

Western blotting

Conventional western blotting was performed to quantify ASC, mature IL-1β, and GSDMD-N. Protein lysates were adjusted to a final concentration of 25 µg protein per 25 µL, mixed with NuPAGE™ LDS Sample Buffer and NuPAGE™ Sample Reducing Agent, and denatured at 90°C for 5 min before electrophoresis. Equal amounts of protein (20 µg) were separated on 4–12% Bis-Tris gradient gels using MES or MOPS running buffer depending on the molecular weight of the target protein and transferred onto PVDF membranes using the XCell II™ Blot Module.

Membranes were blocked in 3% BSA in TBS-T for 1 h at room temperature and incubated overnight at 4°C with primary antibodies diluted in TBS-T containing 3% BSA. After washing, membranes were incubated with species-specific IRDye® 680RD or IRDye® 800CW secondary antibodies for 2 h at room temperature. Membranes were subsequently washed twice in TBS-T and once in TBS

before fluorescence imaging using an Odyssey M® LI-COR imaging system. Fluorescence intensities were quantified using Image Studio™ 4.0 software and normalized to β-actin. Antibody information is summarized in Additional file 1: Table S1.

Automated capillary western immunoassay (Wes)

Automated capillary western immunoassays were performed on a ProteinSimple Wes system. Whole tissue extracts were diluted in 0.1× sample buffer, combined with 5× fluorescent master mix (5× sample buffer, 5× fluorescent standard, 200 mM DTT) at a 4:1 ratio, and denatured at 95 °C for 5 min. The master mix contained three fluorescent internal standards used to align capillaries, since the molecular weight ladder is applied only to the first capillary and each capillary is run independently. These fluorescent standards serve exclusively for capillary alignment and were not used as a loading control. Equal protein input was ensured by BCA-based adjustment of all lysates to an identical concentration, and target signals were additionally normalized to total protein determined by the ProteinSimple total-protein detection module. Denatured samples, blocking reagent, primary antibodies (1:50 for anti-caspase-1 and anti-AIM2), HRP-conjugated secondary antibodies, a biotinylated molecular weight ladder and chemiluminescent substrate were loaded onto the assay plate, after which separation and immunodetection proceeded automatically. Chemiluminescence was recorded as electropherograms using Compass for SimpleWestern software v6.1.0, and the area under each peak was used as a measure of relative protein abundance. Linear dynamic ranges were determined for each target by linear regression. Antibody details are provided in Additional file 1: Table S1.

Immunoprecipitation

To enrich NLRP3 protein complexes, immunoprecipitation was performed using ipsilateral brain lysates. Protein concentrations were adjusted based on the BCA assay, and equal amounts of total protein were diluted in lysis buffer. Protein G Dynabeads™ were pre-incubated with an anti-NLRP3 antibody (2 µg antibody per 25 µL beads) overnight at 4°C under continuous rotation.

Antibody-coupled beads were washed and incubated with protein lysates for 2 h at 4°C under continuous rotation. Following magnetic separation, the flow-through was collected and beads were washed twice with lysis buffer. Bound proteins were eluted in NuPAGE™ LDS Sample Buffer containing Sample Reducing Agent by heating to 95°C for 5 min and subsequently subjected to SDS-PAGE and western blotting as described above. Detailed information on antibodies is provided in Additional file 1: Table S1.

Statistical analysis

Statistical analyses were performed using GraphPad Prism version 10.3 (GraphPad Software, Boston, MA, USA). Normality was assessed using the Shapiro–Wilk test. Infarct volumes, protein abundances and fluorescence intensity ratios are displayed as box plots (median, interquartile range and range) together with the individual animals; group values quoted in the text are given as mean ± standard error of the mean (SEM). Groups were compared using unpaired two-tailed Student's t-tests. Neurological scores are ordinal and are therefore presented as median with range and compared using two-tailed Mann–Whitney U tests, for which exact p values were computed. Quantitative immunofluorescence analyses of ASC-positive cell numbers were analyzed using two-way analysis of variance (two-way ANOVA) followed by Tukey's multiple comparisons test. The ipsilesional-to-contralateral ratio of nanobody-derived ASC fluorescence after ex vivo staining was compared between treatment groups using an unpaired two-tailed Student's t-test. The corresponding ratio for nanobody administered in vivo was obtained from a single cohort without a comparator group and is therefore reported descriptively, without statistical testing. All statistical tests were two-sided, and p values < 0.05 were considered statistically significant. Statistical significance is indicated as $*p < 0.05$, $**p < 0.01$, and $***p < 0.001$. The experimental unit (n) represents individual animals. Exact p values are reported throughout, including for comparisons that did not reach the significance threshold. Group sizes for the primary endpoint were determined by prospective sample size calculation. Assuming a reduction of infarct volume of 30% as functionally relevant and a standard deviation of 20% of the respective mean values, a group size

of eight or more animals was necessary to show this effect with a power of 0.8 and a probability of a type I error of < 0.05 (GraphPad StatMate 2.00). For the secondary biochemical and histological readouts, no separate prospective sample size calculation was performed. For immunofluorescence and conventional western blotting, group sizes were based on those that had yielded robust and reproducible results for the same assays, antibodies and tissue preparations in our previous work using these models [22,23,25]. The automated capillary western immunoassay was newly established for this study, so that no comparable prior experience was available; group sizes were therefore determined by the amount of ipsilesional tissue remaining from the respective cohorts, and the linear dynamic range was verified for each target before quantification. Group sizes for all secondary analyses are stated in the respective figure legends.

Results

VHH(mASC) treatment limits ischemic brain injury during vessel occlusion and following reperfusion

To determine whether targeting ASC provides protection across distinct phases of AIS, VHH(mASC) was evaluated in three complementary treatment paradigms. Mice received the nanobody prophylactically immediately before 4 h pMCAO, therapeutically 1 h after induction of permanent ischemia (1+3 h pMCAO), or immediately after reperfusion following 1 h tMCAO prior to 23 h of reperfusion (1+23 h tMCAO).

Prophylactic administration of VHH(mASC) reduced infarct volume by 61% compared with the control nanobody after 4 h pMCAO (VHH(Inf. A) 74.3 ± 4.8 mm^3; VHH(mASC) 29.0 ± 4.1 mm^3, $p < 0.0001$; Figure 1A,B). Importantly, protection was maintained when treatment was delayed until 1 h after vessel occlusion, reducing infarct volume by 40% (80.4 ± 7.0 mm^3 versus 47.9 ± 7.0 mm^3,

p = 0.006). Sham-operated animals showed no loss of MAP2 immunoreactivity in any paradigm and served as the surgical control (Figure 1B). Therapeutic administration immediately after reperfusion likewise reduced infarct volume by 43% following 1+23 h tMCAO (90.3 ± 9.1 mm^3 versus 51.3 ± 3.4 mm^3, p = 0.001).

The reduction in tissue injury was accompanied by improved neurological function. VHH(mASC) increased the composite neuroscore after 4 h pMCAO (VHH(Inf. A) median 2 [range 1–8], n = 9; VHH(mASC) 6 [2–10], n = 8; p = 0.019), after therapeutic administration during persistent occlusion (2 [1–5], n = 7 versus 4 [2–9], n = 8; p = 0.032), and following ischemia–reperfusion (2 [1–9], n = 7 versus 9 [2–10], n = 8; p = 0.025; Figure 1C). Thus, ASC-directed treatment remained effective when initiated after stroke onset and consistently reduced infarct volume while improving neurological outcome across both persistent vessel occlusion and ischemia–reperfusion paradigms.

VHH(mASC) reaches ischemic brain tissue and reduces cerebral ASC abundance

We next examined whether the therapeutic effects of VHH(mASC) were associated with cerebral exposure to the nanobody and reduced ASC abundance. Fluorescence imaging of brain sections from mice that had received fluorophore-conjugated VHH(mASC) in vivo at 10% of the therapeutic dose revealed punctate nanobody-associated signal within the ipsilesional hemisphere after 4 h pMCAO (n = 5; Figure 2A). Quantified against the contralateral hemisphere of the same section, this signal was enriched 8.9-fold to 12.2-fold within the lesion. Systemically administered nanobody therefore reaches the ischemic lesion.

Consistent with effective targeting of cerebral ASC, VHH(mASC) reduced ASC protein abundance. In cortical tissue, ASC was reduced by 58% following prophylactic treatment during 4 h pMCAO (VHH(Inf. A) 0.446 ± 0.051; VHH(mASC) 0.189 ± 0.029; p = 0.001), by 48% after therapeutic treatment during 1+3 h pMCAO (0.259 ± 0.032 versus 0.134 ± 0.010; p = 0.001), and by 43% following 1+23 h tMCAO (0.178 ± 0.028 versus 0.102 ± 0.020; p = 0.047; Figure 2B). Similar changes were

observed in the basal ganglia, where ASC abundance was significantly reduced following therapeutic treatment both during persistent vessel occlusion (1+3 h pMCAO, p = 0.0001) and after ischemia–reperfusion (1+23 h tMCAO, p = 0.039), while prophylactic treatment showed the same trend without reaching statistical significance (p = 0.130). Ex vivo staining of brain sections with fluorophore-conjugated VHH(mASC) pointed in the same direction. Nanobody-detectable ASC was enriched in the ipsilesional hemisphere of control animals and was markedly lower after VHH(mASC) treatment (ipsilesional-to-contralateral intensity ratio 4.50 ± 0.43 versus 2.26 ± 0.36; p = 0.001; n = 8 per group; Figure 2C), whereas an IgG isotype control showed no specific signal.

ASC-positive cell populations differ between the two ischemic paradigms

Cell-specific analyses revealed a markedly different cellular distribution of ASC between the two paradigms examined. ASC-positive Ly6G-positive neutrophils were already abundant during persistent vessel occlusion and remained detectable following reperfusion. VHH(mASC) reduced their number during both pMCAO (VHH(Inf. A), 10 ± 2 cells; VHH(mASC), 1 ± 0.5 cells per 10 mm^2; p = 0.0001) and tMCAO (13 ± 2 versus 2 ± 0.5 cells per 10 mm^2; p < 0.0001; Figure 3C).

In contrast, microglia and neurons were rarely ASC-positive after 4 h of persistent occlusion but were frequently ASC-positive in the 1+23 h tMCAO condition. ASC/Iba1-double-positive cells increased from 4 ± 0.5 during 4 h pMCAO to 91 ± 7 following tMCAO in control animals. This increase was almost completely prevented by VHH(mASC), which reduced ASC/Iba1-double-positive cells to 4 ± 1 (p < 0.0001; Figure 3A).

A comparable pattern was observed in neurons. ASC/NeuN-double-positive cells increased from 11 ± 1 during 4 h pMCAO to 72 ± 5 following reperfusion in VHH(Inf. A)-treated mice. This increase was almost completely prevented by VHH(mASC), reducing ASC/NeuN-double-positive cells to 5 ± 1 (p < 0.0001; Figure 3B).

ASC-positive neutrophils were present during persistent occlusion and changed little thereafter, whereas ASC-positive microglia and neurons were approximately 23-fold and 6.5-fold more numerous, respectively, in the 1+23 h tMCAO condition than after 4 h pMCAO.

VHH(mASC) suppresses convergent inflammasome activation and downstream pyroptotic signaling

Having established cerebral target engagement and neuroprotection, we next examined whether ASC-directed treatment interfered with multiple inflammasome pathways and their shared downstream effectors.

VHH(mASC) reduced cortical AIM2 abundance by 40% following prophylactic treatment during 4 h pMCAO (p = 0.045; Figure 4A). AIM2 was also reduced by 28% following ischemia–reperfusion (p = 0.047). A numerical reduction of 26% was observed after therapeutic treatment during pMCAO but narrowly failed to reach statistical significance (p = 0.051). To determine whether targeting ASC also affected the best-characterized inflammasome pathway in stroke, NLRP3 was enriched by immunoprecipitation. VHH(mASC) reduced immunoprecipitated NLRP3 by 30% following prophylactic treatment (4 h pMCAO; p = 0.015) and by 24% following therapeutic treatment during permanent artery occlusion (1+3 h pMCAO; p = 0.037). A comparable numerical reduction of 23% following 1+23 h tMCAO did not reach statistical significance (p = 0.070; Figure 4B). These findings indicate that ASC-directed treatment affects more than one upstream inflammasome pathway.

Pro-caspase-1 abundance was not significantly altered by treatment, but showed a consistent numerical increase in VHH(mASC)-treated animals in all three paradigms (4 h pMCAO, p = 0.105; 1+3 h pMCAO, p = 0.419; 1+23 h tMCAO, p = 0.071; Figure 4C). In contrast, VHH(mASC) reduced the abundance of cleaved caspase-1 across all treatment paradigms (4 h pMCAO, p = 0.017; 1+3 h pMCAO, p = 0.002; 1+23 h tMCAO, p = 0.009; Figure 4D).

Similarly, mature IL-1β abundance was consistently reduced in ipsilesional cortical tissue across all treatment paradigms (4 h pMCAO, $p = 0.008$; 1+3 h pMCAO, $p = 0.048$; 1+23 h tMCAO, $p = 0.012$; Figure 4E). The same was observed in the basal ganglia after therapeutic treatment during persistent vessel occlusion ($p = 0.048$) and after ischemia–reperfusion ($p = 0.047$), whereas prophylactic treatment showed a comparable trend that did not reach statistical significance ($p = 0.065$). Consistent with these findings, VHH(mASC) also reduced the N-terminal pyroptotic effector fragment GSDMD-N across all treatment paradigms (4 h pMCAO, $p = 0.003$; 1+3 h pMCAO, $p = 0.002$; 1+23 h tMCAO, $p = 0.031$; Figure 4F).

Together, VHH(mASC) reduced the abundance of both AIM2 and immunoprecipitated NLRP3, while leaving pro-caspase-1 abundance unchanged. In contrast, cleaved caspase-1, mature IL-1β, and GSDMD-N were reduced across treatment paradigms, indicating broad suppression of downstream inflammasome signaling.

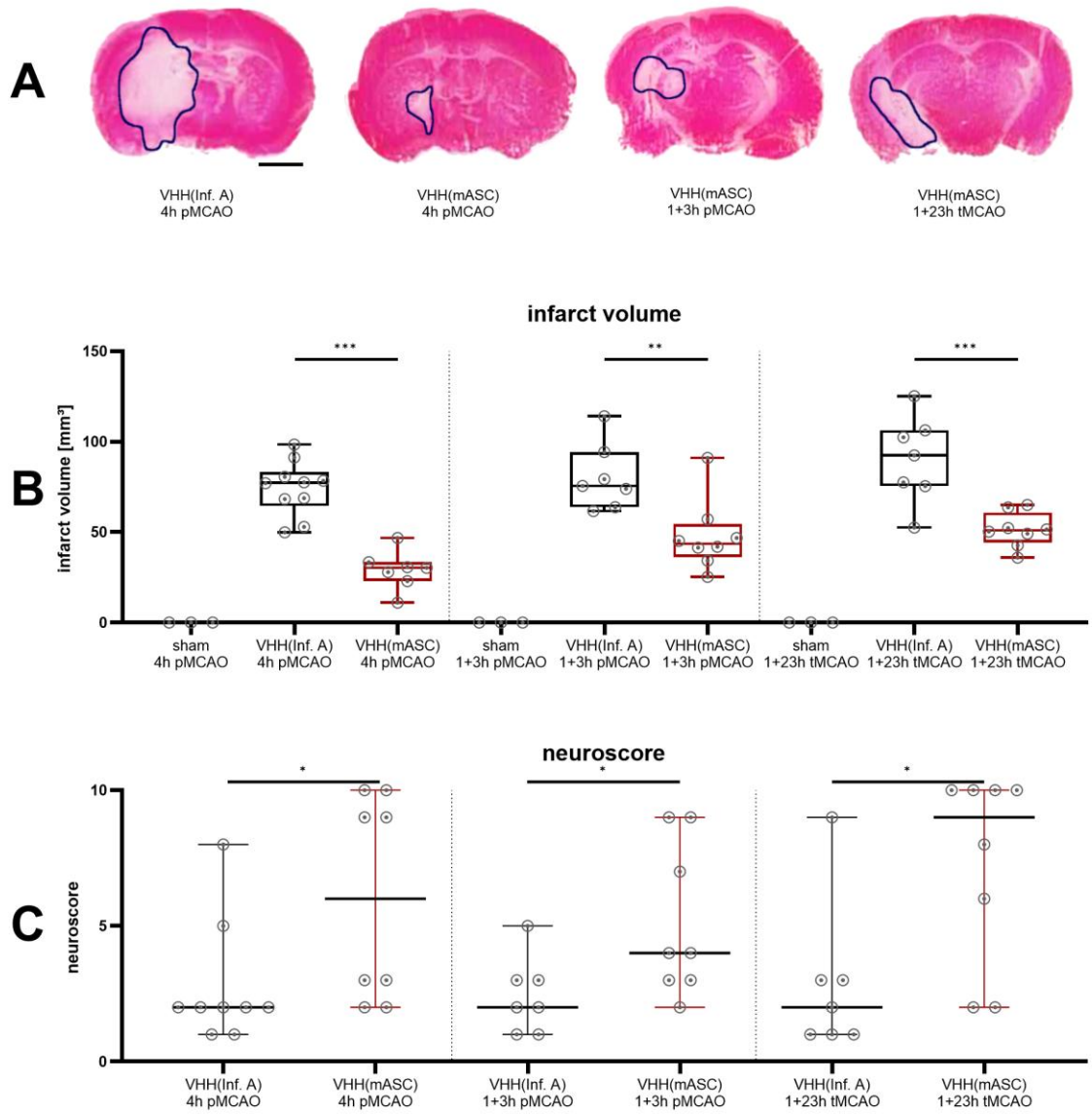


Figure 1. VHH(mASC) nanobody treatment reduces infarct volume and improves neurological outcome following experimental ischemic stroke.

(A) Representative MAP2-stained coronal brain sections illustrating infarct demarcation after experimental ischemic stroke. Infarct areas are outlined in blue. Shown are representative sections from mice receiving the inert control nanobody VHH(Inf. A) or prophylactic VHH(mASC) treatment and subjected to 4 h permanent middle cerebral artery occlusion (pMCAO), therapeutic VHH(mASC) treatment initiated 1 h after stroke onset followed by 3 h pMCAO (1+3 h pMCAO), and therapeutic VHH(mASC) treatment initiated 1 h after transient middle cerebral artery occlusion followed by 23 h reperfusion (1+23 h tMCAO). Scale bar = 2 mm.

(B) Quantification of infarct volume. VHH(mASC) reduced infarct volume compared with VHH(Inf. A) in all treatment paradigms. Sham-operated animals, which underwent the identical procedure without advancing the filament, are shown for each paradigm and had no measurable infarct; n = 3 per paradigm.

(C) Neurological deficits assessed using the composite neuroscore. VHH(mASC) improved neurological function compared with VHH(Inf. A).

Infarct volumes in (B) are shown as box plots (median, interquartile range and range) together with individual animals and were compared using unpaired two-tailed Student's t-tests. Because the composite neuroscore is an ordinal variable, neuroscores in (C) are deliberately not displayed as box plots but as individual values with median and range, and were compared using two-tailed Mann–Whitney U tests; n = 7–9. *p < 0.05, **p < 0.01, ***p < 0.001.

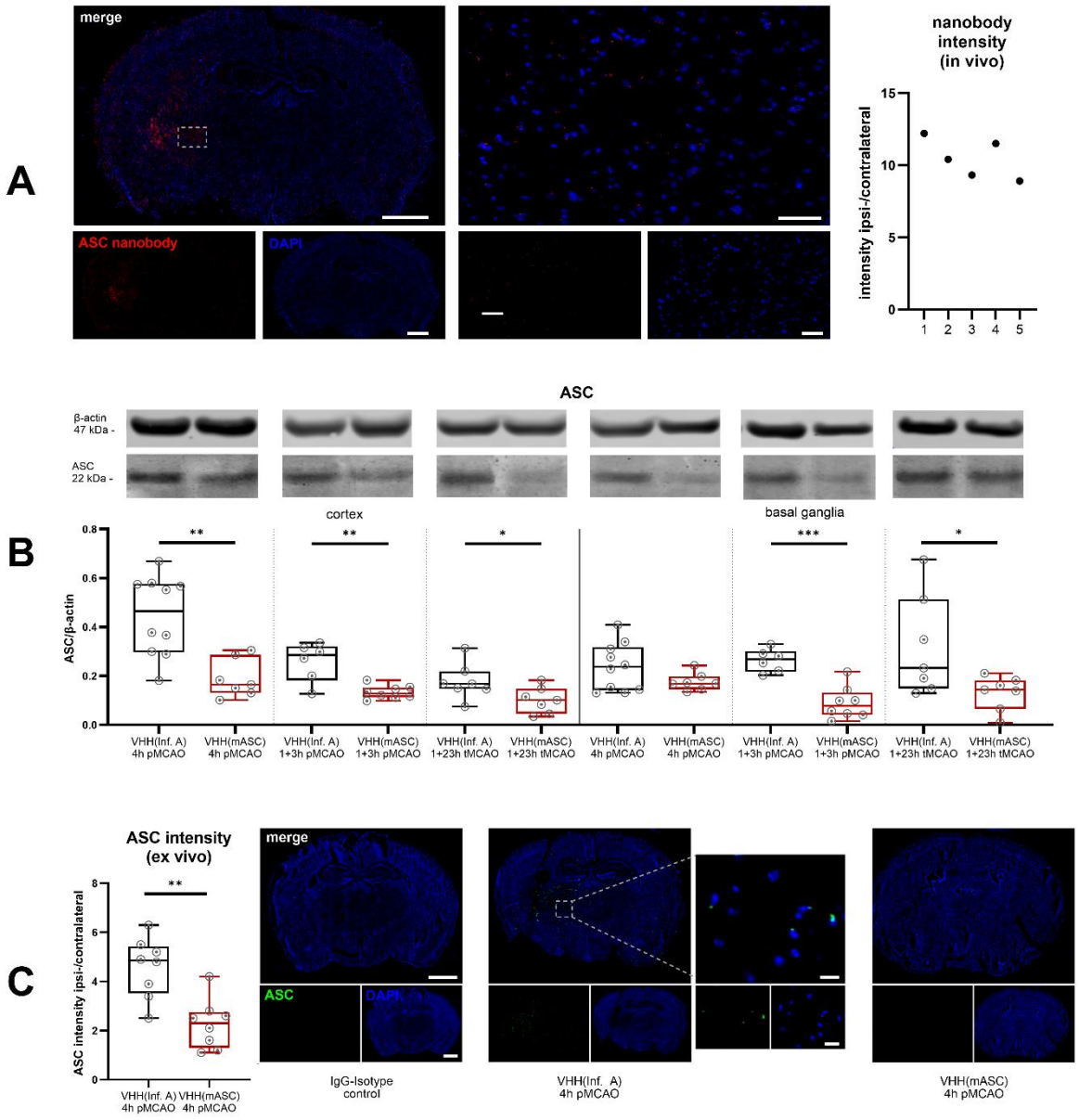


Figure 2. VHH(mASC) reaches ischemic brain tissue and reduces cerebral ASC abundance.

(A) Representative fluorescence images of ipsilesional brain tissue from mice that received Alexa Fluor™ 488-conjugated VHH(mASC) in vivo at 10% of the therapeutic dose (0.5 µg/g body weight) immediately before 4 h permanent

middle cerebral artery occlusion (pMCAO). The Alexa Fluor™ 488 signal was acquired in its corresponding channel and is deliberately displayed in red by assigning a red lookup table at the microscope, so that nanobody administered in vivo is visually distinct from the ex vivo nanobody staining shown in green in (C). Nanobody-associated signal (red) is therefore shown as a merge with DAPI (blue) and as separate channels; the boxed region is shown at higher magnification on the right. Sections were imaged directly, without additional ASC immunostaining. Quantification on the right shows the mean fluorescence intensity of the nanobody-derived signal, expressed as the ratio of the ipsilesional to the contralateral hemisphere of the same section; each symbol represents one animal (n = 5). As this cohort comprised a single group, no statistical comparison was performed. For the same reason the values in (A) are shown as individual animals without a box plot, in contrast to the group comparisons in (B) and (C). Images are representative of these five animals. Scale bar = 2 mm (overview); 100 µm (inset).

(B) Representative western blots and corresponding quantification of ASC protein abundance normalized to β-actin in ipsilesional cortical and basal ganglia tissue following prophylactic and therapeutic VHH(mASC) treatment; n = 6–10.

(C) Representative fluorescence images of nanobody-detectable ASC. Cryosections from mice treated with VHH(Inf. A) or with VHH(mASC) at the therapeutic dose during 4 h pMCAO were stained ex vivo with Alexa Fluor™ 488-conjugated VHH(mASC) (green) and counterstained with DAPI (blue); an IgG isotype control was processed in parallel to confirm staining specificity. Merge and separate channels are shown, with the boxed region at higher magnification. Quantification on the left shows the mean fluorescence intensity of the nanobody-derived ASC signal, expressed as the ratio of the ipsilesional to the contralateral hemisphere of the same section; n = 8 per group. Scale bar = 2 mm (overview); 50 µm (inset).

Quantitative data in (B) and (C) are shown as box plots (median, interquartile range and range) together with individual animals and were compared using unpaired two-tailed Student's *t*-tests. $*p < 0.05$, $**p < 0.01$, $***p < 0.001$.

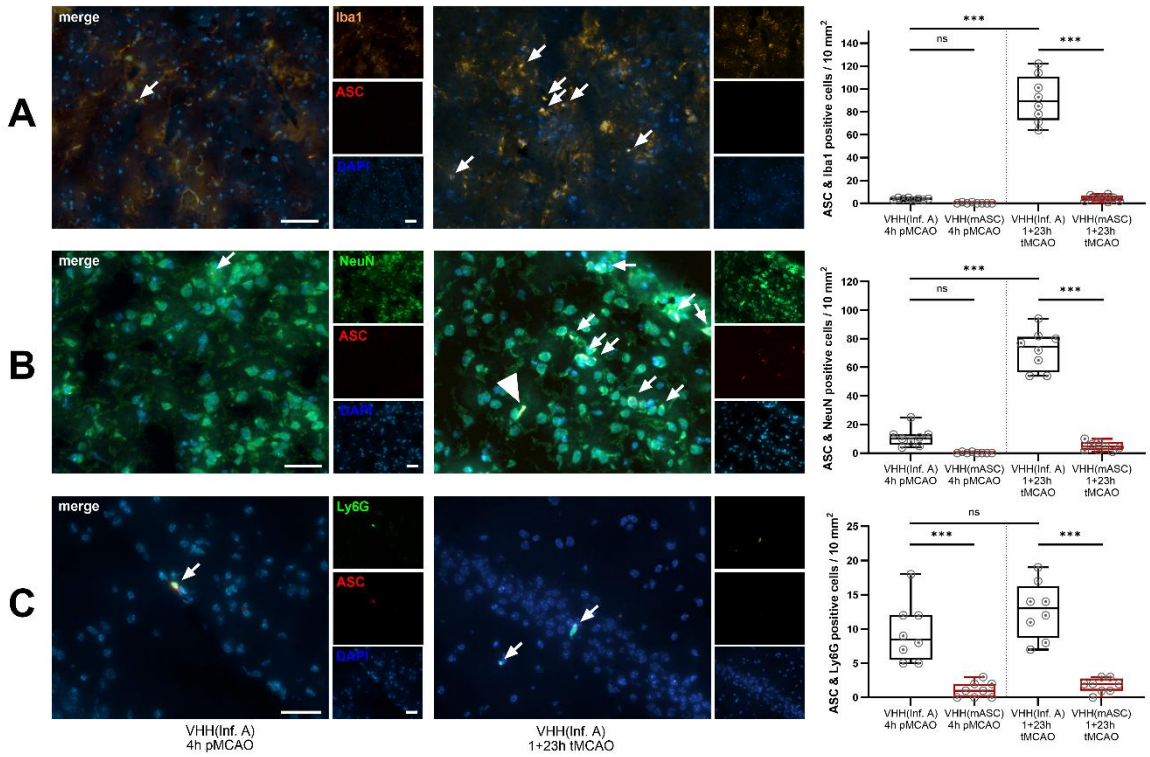


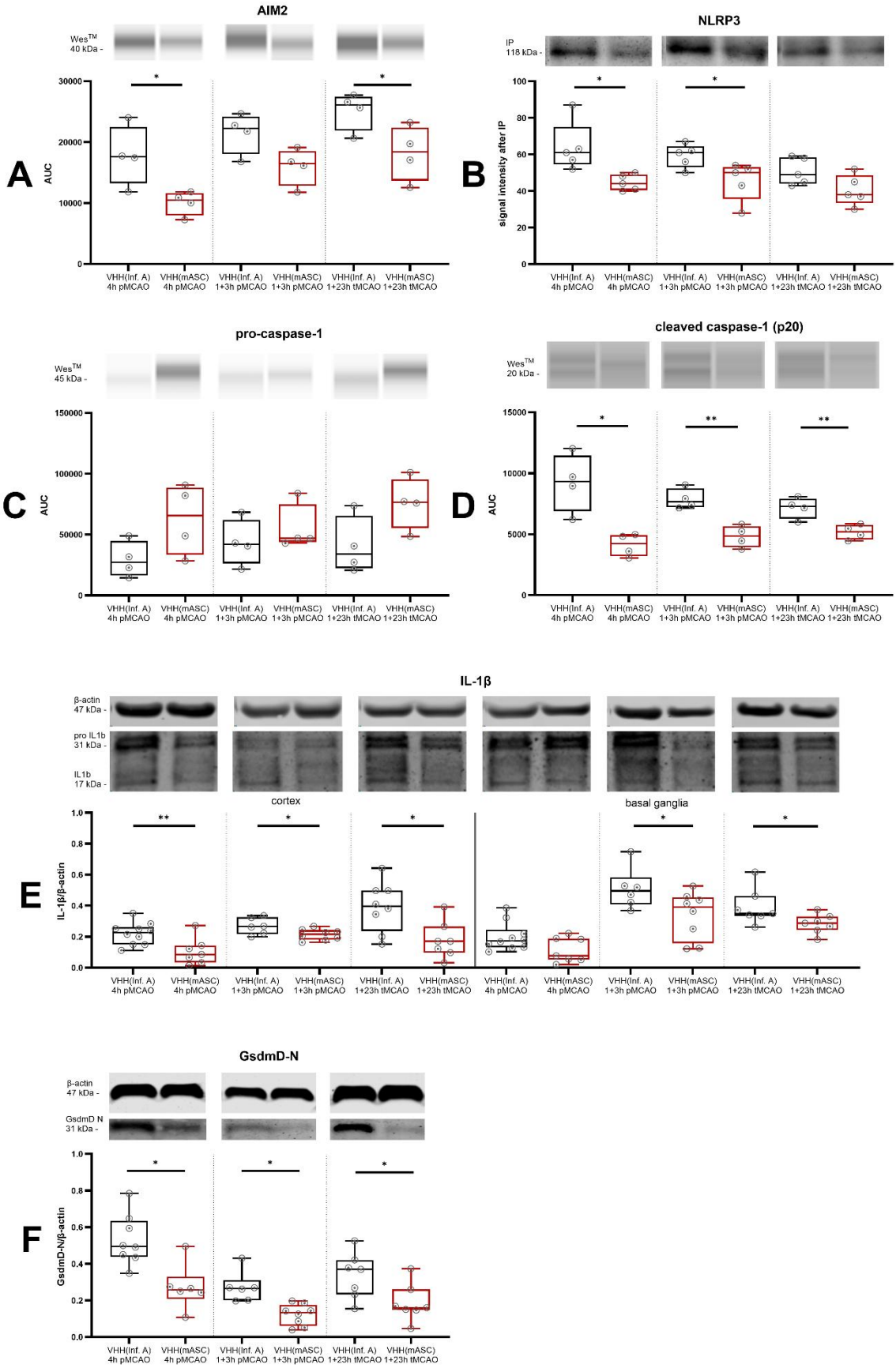
Figure 3. Cellular distribution of ASC differs between ischemic paradigms and is reduced by VHH(mASC) nanobody treatment.

(A) Representative immunofluorescence staining of ASC (red) and the microglial marker Iba1 (orange) in the ipsilesional penumbra after 4 h permanent middle cerebral artery occlusion (pMCAO) and after 1+23 h transient middle cerebral artery occlusion (tMCAO). Merge and separate channels are shown. Arrows indicate representative ASC-positive microglia. Quantification of ASC/Iba1-double-positive cells per 10 mm^2 is shown on the right; n = 8. Scale bar = 100 µm.

(B) Representative immunofluorescence staining of ASC (red) and the neuronal marker NeuN (green) in the ipsilesional penumbra after 4 h pMCAO and after 1+23 h tMCAO. Arrows indicate representative ASC-positive neurons. The arrowhead indicates extracellular ASC immunoreactivity adjacent to a morphologically degenerating neuron. Quantification of ASC/NeuN-double-positive cells per 10 mm^2 is shown on the right; n = 8. Scale bar = 100 µm.

(C) Representative immunofluorescence staining of ASC (red) and the neutrophil marker Ly6G (green) in the ipsilesional penumbra after 4 h pMCAO and after 1+23 h tMCAO. Arrows indicate representative ASC-positive Ly6G-positive neutrophils. Quantification of ASC/Ly6G-double-positive cells per 10 mm^2 is shown on the right; n = 8. Scale bar = 100 µm.

Cell counts are expressed per 10 mm^2 and are shown as box plots (median, interquartile range and range) together with individual animals. Representative images were selected for image quality only and do not define the region used for quantification. Comparisons were performed using two-way ANOVA followed by Tukey's multiple comparisons test. ns, not significant; *$p < 0.05$, **$p < 0.01$, ***$p < 0.001$.


AIM2
Wes™
40 kDa -
A
AUC
VHH(Inf. A) 4h pMCAO
VHH(mASC) 4h pMCAO
VHH(Inf. A) 1+3h pMCAO
VHH(mASC) 1+3h pMCAO
VHH(Inf. A) 1+23h tMCAO
VHH(mASC) 1+23h tMCAO
NLRP3
IP
118 kDa -
B
signal intensity after IP
pro-caspase-1
Wes™
45 kDa -
C
AUC
cleaved caspase-1 (p20)
Wes™
20 kDa -
D
AUC
IL-1β
β-actin
47 kDa -
pro IL1b
31 kDa -
IL1b
17 kDa -
cortex
basal ganglia
E
IL-1β/β-actin
GsdmD-N
β-actin
47 kDa -
GsdmD N
31 kDa -
F
GsdmD-N/β-actin

530

Figure 4. VHH(mASC) nanobody treatment suppresses convergent inflammasome activation and downstream pyroptotic signaling following experimental ischemic stroke.

(A) Representative Wes electropherograms and corresponding quantification (AUC: area under the curve) of absent in melanoma 2 (AIM2) protein abundance in ipsilesional cortical tissue following prophylactic treatment during 4 h permanent middle cerebral artery occlusion (pMCAO), therapeutic treatment during 1+3 h pMCAO, and therapeutic treatment following 1+23 h transient middle cerebral artery occlusion (tMCAO); n = 4.

(B) Representative NLRP3 immunoprecipitation and corresponding densitometric quantification in ipsilesional cortical tissue; n = 5.

(C) Representative Wes electropherograms and corresponding quantification of pro-caspase-1 (pro-Csp1) protein abundance in ipsilesional cortical tissue; n = 4.

(D) Representative Wes electropherograms and corresponding quantification of cleaved caspase-1 (Csp1 p20) protein abundance in ipsilesional cortical tissue; n = 4.

(E) Representative western blots and corresponding densitometric quantification of mature interleukin-1β (IL-1β) normalized to β-actin in ipsilesional cortical and basal ganglia tissue; n = 6–10.

(F) Representative western blots and corresponding densitometric quantification of the N-terminal cleavage fragment of gasdermin D (GSDMD-N) normalized to β-actin in ipsilesional cortical tissue; n = 6–10.

Quantitative data are shown as box plots (median, interquartile range and range) together with individual animals and were compared using unpaired two-tailed Student's t-tests. *$p < 0.05$, **$p < 0.01$, ***$p < 0.001$.

Discussion

Pharmacological targeting of ASC using a camelid-derived nanobody conferred neuroprotection during both the hyperacute phase in AIS (pMCAO) and after reperfusion (tMCAO). VHH(mASC) reduced infarct volume and improved neurological outcome in all three treatment paradigms. Mechanistically, treatment reduced cerebral ASC abundance, lowered the abundance of both NLRP3 and AIM2, and suppressed the downstream effector cascade comprising caspase-1 activation, IL-1β maturation and GSDMD cleavage, all of which moved concordantly in each paradigm. This consistency across independent readouts and ischemic conditions argues against a paradigm-specific effect, as does the use of an inert influenza A-specific nanobody as comparator, which controls for protein load, injection and non-specific VHH effects. Labeled nanobody

given in vivo was enriched within the lesion relative to the contralateral hemisphere. Neuroprotective agents have repeatedly entered clinical testing without evidence that they reach ischemic brain tissue; for VHH(mASC), that evidence now exists. Together, these readouts trace a coherent pharmacological chain from administered nanobody to its target and on to outcome, and they converge with independent genetic evidence that ASC deficiency limits acute ischemic brain injury [26]. A binding-deficient VHH variant and a Pycard-deficient arm would convert this convergent evidence into formal proof of ASC dependence.

Our findings extend the current concept of inflammasome-directed stroke therapy. Most experimental approaches have focused on inhibiting individual inflammasome sensors, particularly NLRP3 [13,15–17]. ASC inhibition instead targets the common adaptor required for multiple canonical inflammasomes and therefore acts downstream of, and independently of, any individual upstream sensor [7]. Sensor-level inhibition has meanwhile reached clinical testing, with an oral NLRP3 inhibitor meeting its primary inflammation endpoint in individuals at elevated cardiovascular risk [27]. In the same laboratory, and with the same surgical procedure, infarct readout and neuroscore, selective NLRP3 inhibition reduced infarct volume by approximately 25–40% in both paradigms used here [5,13]. Adaptor-level inhibition therefore performs at or above the upper end of what sensor-specific intervention has achieved under comparable conditions, although separate cohorts rather than a contemporaneous randomized comparison make this a quantitative indication rather than a formal superiority claim.

The relative contribution of individual ASC-dependent inflammasomes is unlikely to remain static during lesion evolution [19,28,29]. In our previous work, transient cerebral ischemia induced NLRP3 strongly, whereas AIM2 and NLRP1 responded more modestly; pharmacological NLRP3 inhibition was nevertheless protective across paradigms, identifying NLRP3 as a major but not exclusive driver of post-ischemic inflammasome activation [13]. Additional ASC-dependent

inflammasomes, including AIM2, NLRC4 and NLRP1, have likewise been implicated in experimental ischemic brain injury [26,29]. Sensor-specific inhibition therefore depends on correctly identifying the dominant inflammasome at a given stage of disease, whereas adaptor-level inhibition does not. Consistent with this, VHH(mASC) lowered both NLRP3 and AIM2 in the same animals.

The reduction of AIM2 deserves comment, since independent studies have linked this sensor to acute tissue damage and to post-stroke cognitive impairment [20,26,30]. AIM2 is activated by cytosolic double-stranded DNA released during ischemic cell injury, so its abundance partly tracks ongoing cellular disruption, and a contribution of reduced overall tissue injury to both sensor readouts cannot be excluded. The concordant reduction of ASC itself, however, is the expected consequence of engaging the shared adaptor rather than of a smaller lesion alone.

The mode of action of ASC-directed nanobodies may explain this breadth. Unlike small molecules that prevent activation of individual sensors, extracellularly administered VHH(mASC) preferentially targets polymerized ASC after pyroptotic membrane permeabilization or extracellular release. VHH(mASC) binds the pyrin domain (PYD) of murine ASC, through which ASC molecules polymerize with one another, and thus engages the interface between ASC molecules rather than that between ASC and an upstream sensor. Structural work on full-length ASC indicates that specks are built from bundles of alternating PYD and CARD filaments, and that disrupting either interface abolishes speck formation and caspase-1 activation [31]. Masking these contacts shifts assembled ASC towards monomers, which explains why the nanobody disassembles preformed specks rather than merely preventing their nucleation, and why it interrupts their prionoid propagation while largely preserving initial, cell-intrinsic IL-1β responses. Because tissue-level readouts capture both primary and speck-propagated inflammasome activity, the reductions in caspase-1 cleavage, IL-1β maturation and GSDMD cleavage observed here are compatible with

such preservation. The caspase-1 data carry a pharmacodynamic signature of this mode of action. Pro-caspase-1 was preserved, with a consistent numerical increase in treated animals, while the cleaved p20 fragment fell in every paradigm. Treatment therefore interferes with proteolytic processing of the zymogen at the ASC platform, where pro-caspase-1 is recruited and activated by induced proximity, rather than with caspase-1 expression. This dissociation also argues against reduced lesion size as a sufficient explanation of the biochemical findings, since a smaller lesion would be expected to lower the zymogen and its cleavage product together.

This mechanism also bears on which cells were affected. ASC positivity was largely confined to infiltrating neutrophils at the early time point under persistent occlusion and was prominent in microglia and neurons at the later time point after reperfusion, and VHH(mASC) reduced it in all three compartments. This distribution is not confined to the mouse: in thrombi retrieved by mechanical thrombectomy from patients with large-vessel occlusion, the majority of intrathrombotic neutrophils carry ASC, including visible specks [32]. An extracellularly acting nanobody does not need to enter a particular cell type in order to be effective, because it engages ASC once membrane integrity is lost or ASC has been released; coverage across cellular compartments is therefore an expected property of this mechanism rather than an additional assumption, and it distinguishes the approach from intracellular inhibitors, whose effect depends on uptake into the relevant cell. We would further propose that these compartments are not independent. ASC specks released from neutrophils dying early in the lesion are plausible seeds for inflammasome activation in resident brain cells, in keeping with the prionoid activity of extracellular ASC [12] and with the finding that extracellular ASC aggravates ischemic injury [33]. Whether the later resident-cell response depends on this earlier neutrophil-derived signal remains to be tested, for example by depleting neutrophils before treatment.

Post-pyroptotic targeting may also confer a favorable immunological profile. Extracellular ASC specks released from pyroptotic cells remain accessible to the nanobody, whereas intact cells do not. Two features of the molecule argue against broad immunosuppression: VHH(mASC) lacks an Fc domain and therefore cannot promote Fc receptor-mediated uptake or effector functions, and it does not efficiently cross intact plasma membranes, so inflammasome assembly in non-pyroptotic cells should remain under physiological control. ASC is already being pursued as a drug target with a humanized full-length IgG4 antibody, which is protective in preclinical models of multiple sclerosis, traumatic brain injury and Parkinson disease but has not been reported in cerebral ischemia [34,35]. The nanobody format differs from that approach in carrying no Fc region and in acting on ASC that has already polymerized. Whether repeated or prolonged treatment affects antimicrobial defense has not been tested here and would require dedicated infection models; given the single-dose, short-course regimen used in acute stroke, this is a limitation of scope rather than an immediate safety concern.

Several boundaries define what these data can and cannot support. Our mechanistic analyses addressed NLRP3 and AIM2, the ASC-dependent sensors with the strongest prior evidence in cerebral ischemia; this follows from the strategy rather than being an omission, since adaptor-level inhibition should act irrespective of which sensor dominates. What the design does not resolve is the relative contribution of the two mechanisms available to VHH(mASC), inhibition of canonical inflammasome signaling and interruption of extracellular ASC speck propagation. Readouts were placed at the protein level, where inflammasome signaling is regulated [7]. Cerebral nanobody concentrations were not quantified, and the labeled nanobody was imaged at a reduced dose and without an identically labeled control, so the intensity ratio documents enrichment within the lesion but establishes neither binding specificity nor concentration under therapeutic dosing; lesion-restricted access is arguably desirable for a target that resides where the blood–brain barrier is already compromised, but formal pharmacokinetic characterization remains outstanding.

Finally, experiments were performed in young healthy male mice; validation in aged animals, females and models with vascular comorbidities, together with delayed treatment and long-term outcomes, will be required before clinical translation.

Several steps follow directly from this work. The loss-of-function arm named above requires a parallel wild-type cohort, since ASC deficiency is itself protective [26]. Clinically, the efficacy observed under both ischemic conditions has a practical implication: because protection did not depend on whether the vessel was reopened, ASC-directed treatment would not require knowing in advance whether recanalization will succeed, and could in principle be started before that outcome is determined — including before admission, when the inflammatory cascade is already running and no specific treatment is yet available. The present experiments nevertheless establish efficacy only at early treatment and outcome time points, and future studies should define the therapeutic window by delaying treatment for several hours and determine whether acute neuroprotection translates into sustained benefit, which is particularly relevant because inflammasome-dependent lesion progression may remain accessible beyond the hyperacute phase [16]. Finally, the target doubles as a candidate biomarker: circulating ASC and extracellular ASC specks could support both patient stratification and pharmacodynamic monitoring [12]. Single-molecule assays now count ASC specks in human serum and cerebrospinal fluid and separate patients from controls in neurodegenerative disease [36], so the measurement is available; their relationship to cerebral inflammasome activation in stroke and to treatment response is undefined.

Taken together, these data point beyond a single molecule. The only established disease-modifying treatment in acute ischemic stroke is restoring perfusion, and the present approach is aimed at that same acute phase: ASC-directed treatment protected tissue whether or not the vessel was reopened. It also shifts the underlying logic. Rather than preventing a sensor from being activated, the nanobody dismantles a structure that has already assembled and acts on material already

released from dying cells. Because that material persists, benefit may extend beyond the hyperacute window — ASC deficiency limits sustained neuroinflammation and cognitive impairment for weeks after closed-head injury [37] — a possibility we will pursue in a dedicated follow-up study. Adaptor-level targeting with a camelid single-domain nanobody is therefore a mechanistically distinct class of anti-inflammatory intervention rather than an incremental improvement on sensor inhibition. VHH(mASC) is murine-specific, but a human ASC-reactive nanobody that disassembles ASC specks in human cells has already been characterized [21]; establishing its efficacy in cerebral ischemia follows directly from this work.

Conclusion

ASC-directed nanobody treatment reduced infarct volume and improved neurological outcome in two complementary models of ischemic stroke, during persistent vessel occlusion as well as after reperfusion, and did so with demonstrable cerebral target engagement. Targeting the shared adaptor rather than an individual sensor therefore offers protection that is not contingent on inhibiting the dominant sensor, nor on whether recanalization succeeds — a property that distinguishes this approach from sensor-specific inhibition.

Supplementary Information

Additional file 1: Table S1. Antibodies and detection reagents used in this study. Table S2. Critical reagents used in this study.

Additional file 2: Uncropped raw images of all western blots and of the capillary western immunoassay electropherograms shown in Figures 2 and 4.

List of abbreviations

AIM2: absent in melanoma 2; AIS: acute ischemic stroke; ANOVA: analysis of variance; ARRIVE: Animal Research: Reporting of In Vivo Experiments; ASC: apoptosis-associated speck-like protein containing a caspase recruitment domain; ATP: adenosine triphosphate; AUC: area under the curve; BCA: bicinchoninic acid; BSA: bovine serum albumin; CARD: caspase recruitment domain; DAPI: 4',6-diamidino-2-phenylindole; DNA: deoxyribonucleic acid; DTT: dithiothreitol; GSDMD: gasdermin D; GSDMD-N: N-terminal cleavage fragment of gasdermin D; HRP: horseradish peroxidase; IgG: immunoglobulin G; IL: interleukin; IP: immunoprecipitation; LDS: lithium dodecyl sulfate; MAP2: microtubule-associated protein 2; MCA: middle cerebral artery; MES: 2-(N-morpholino)ethanesulfonic acid; MOPS: 3-(N-morpholino)propanesulfonic acid; NLRC4: NLR family CARD domain-containing protein 4; NLRP1: NLR family pyrin domain-containing 1; NLRP3: NLR family pyrin domain-containing 3; PBS: phosphate-buffered saline; pMCAO: permanent middle cerebral artery occlusion; PVDF: polyvinylidene difluoride; PYD: pyrin domain; SDS-PAGE: sodium dodecyl sulfate polyacrylamide gel electrophoresis; SEM: standard error of the mean; TBS: Tris-buffered saline; TBS-T: Tris-buffered saline with Tween 20; tMCAO: transient middle cerebral artery occlusion; VHH: variable domain of a heavy-chain-only antibody (single-domain antibody, nanobody); Wes: automated capillary western immunoassay.

Declarations

Ethics approval and consent to participate

All animal experiments were approved by the Government of Lower Franconia (Regierung von Unterfranken, Würzburg, Germany; approval number 2-2118). All experiments were performed in accordance with the approved protocol, with institutional guidelines and regulations, and with the ARRIVE recommendations. This study did not involve human participants, human data or human tissue; consent to participate is therefore not applicable.

Consent for publication

Not applicable.

Availability of data and materials

All data generated or analysed during this study are included in this published article and its supplementary information files; further datasets are available from the corresponding author on reasonable request. The datasets used and/or analysed during the current study are available from the corresponding author on reasonable request. This study did not generate new unique reagents; the ASC-specific and control nanobodies are available from the laboratory of F.I.S. (Institute of Innate Immunity, University of Bonn) under a material transfer agreement. This paper does not report original code.

Competing interests

The authors declare that they have no competing interests.

Funding

This research was funded by the Else-Kröner-Fresenius-Stiftung (EKFS; 2023_EKEA.187 to M.B.), by the Interdisciplinary Center for Clinical Research (IZKF) at the University of Würzburg (INTERACT 01EO21-A5 to M.B.) and by the HORIZON Lump Sum Grant (ERC PoC UNBIAS, 101123144 to B.S.F.). None of the funders had any role in the conceptualization or design of the study, in data collection, analysis or interpretation, in the decision to publish, or in the preparation of the manuscript.

Authors' contributions

M.B. and B.S.F. conceived and supervised the study. M.B. and M.S. performed the stroke surgeries, neurological assessments, histological and biochemical analyses, and analyzed the data. L.R. and S.M. contributed to the biochemical analyses. F.I.S. generated and provided the ASC-

specific and control nanobodies and the fluorescently conjugated nanobody. M.S. and M.B. prepared the figures and wrote the original draft. All authors read and approved the final manuscript.

Acknowledgements

We thank Hai Yen Hagn and Philomena Schmidt for excellent technical assistance. Moreover, we thank Matilde B. Vasconcelos and Alesja Dernst for their continuous scientific advice.

Authors' information

Not applicable.

References

1. Goyal M, Menon BK, van Zwam WH, Dippel DWJ, Mitchell PJ, Demchuk AM, et al. Endovascular thrombectomy after large-vessel ischaemic stroke: a meta-analysis of individual patient data from five randomised trials. The Lancet. 2016;387:1723–31. https://doi.org/10.1016/S0140-6736(16)00163-X

2. Baron J-C. Protecting the ischaemic penumbra as an adjunct to thrombectomy for acute stroke. Nat Rev Neurol. 2018;14:325–37. https://doi.org/10.1038/s41582-018-0002-2

3. Iadecola C, Anrather J. The immunology of stroke: from mechanisms to translation. Nat Med. 2011;17:796–808. https://doi.org/10.1038/nm.2399

4. Stoll G, Schuhmann MK, Nieswandt B, Kollikowski AM, Pham M. An intravascular perspective on hyper-acute neutrophil, T-cell and platelet responses: Similarities between human and experimental stroke. J Cereb Blood Flow Metab. 2022;0271678X2211057. https://doi.org/10.1177/0271678X221105764

789 5. Bellut M, Kollikowski AM, Vogt ML, Rossnagel L, Hawwari I, Franklin BS, et al. Identifying the
790 role of NLRP3 inflammasome in stroke progression and outcome before recanalization. Cell Re-
791 ports Medicine. 2026;7:102723. https://doi.org/10.1016/j.xcrm.2026.102723

792 6. Eltzschig HK, Eckle T. Ischemia and reperfusion—from mechanism to translation. Nat Med.
793 2011;17:1391–401. https://doi.org/10.1038/nm.2507

794 7. Lamkanfi M, Dixit VM. Mechanisms and Functions of Inflammasomes. Cell. 2014;157:1013–
795 22. https://doi.org/10.1016/j.cell.2014.04.007

796 8. Broz P, Dixit VM. Inflammasomes: mechanism of assembly, regulation and signalling. Nat Rev
797 Immunol. 2016;16:407–20. https://doi.org/10.1038/nri.2016.58

798 9. Shi J, Zhao Y, Wang K, Shi X, Wang Y, Huang H, et al. Cleavage of GSDMD by inflammatory
799 caspases determines pyroptotic cell death. Nature. 2015;526:660–5.
800 https://doi.org/10.1038/nature15514

801 10. Franklin BS, Latz E, Schmidt FI. The intra- and extracellular functions of ASC specks. Immu-
802 nological Reviews. 2018;281:74–87. https://doi.org/10.1111/imr.12611

803 11. Lu A, Magupalli VG, Ruan J, Yin Q, Atianand MK, Vos MR, et al. Unified Polymerization Mecha-
804 nism for the Assembly of ASC-Dependent Inflammasomes. Cell. 2014;156:1193–206.
805 https://doi.org/10.1016/j.cell.2014.02.008

806 12. Franklin BS, Bossaller L, De Nardo D, Ratter JM, Stutz A, Engels G, et al. The adaptor ASC has
807 extracellular and “prionoid” activities that propagate inflammation. Nat Immunol. 2014;15:727–
808 37. https://doi.org/10.1038/ni.2913

809 13. Franke M, Bieber M, Kraft P, Weber ANR, Stoll G, Schuhmann MK. The NLRP3 inflammasome
810 drives inflammation in ischemia/reperfusion injury after transient middle cerebral artery

811 occlusion in mice. Brain, Behavior, and Immunity. 2020;S0889159120324521.
812 https://doi.org/10.1016/j.bbi.2020.12.009

813 14. Swanson KV, Deng M, Ting JP-Y. The NLRP3 inflammasome: molecular activation and regula-
814 tion to therapeutics. Nat Rev Immunol. 2019;19:477–89. https://doi.org/10.1038/s41577-019-
815 0165-0

816 15. Ismael S, Zhao L, Nasoohi S, Ishrat T. Inhibition of the NLRP3-inflammasome as a potential
817 approach for neuroprotection after stroke. Sci Rep. 2018;8:5971.
818 https://doi.org/10.1038/s41598-018-24350-x

819 16. Bellut M, Bieber M, Kraft P, Weber ANR, Stoll G, Schuhmann MK. Delayed NLRP3 inflam-
820 masome inhibition ameliorates subacute stroke progression in mice. J Neuroinflammation.
821 2023;20:4. https://doi.org/10.1186/s12974-022-02674-w

822 17. Abulafia DP, de Rivero Vaccari JP, Lozano JD, Lotocki G, Keane RW, Dietrich WD. Inhibition of
823 the Inflammasome Complex Reduces the Inflammatory Response after Thromboembolic Stroke
824 in Mice. J Cereb Blood Flow Metab. 2009;29:534–44. https://doi.org/10.1038/jcbfm.2008.143

825 18. Fann DY-W, Lim Y-A, Cheng Y-L, Lok K-Z, Chunduri P, Baik S-H, et al. Evidence that NF-κB and
826 MAPK Signaling Promotes NLRP Inflammasome Activation in Neurons Following Ischemic
827 Stroke. Mol Neurobiol. 2018;55:1082–96. https://doi.org/10.1007/s12035-017-0394-9

828 19. Poh L, Kang S-W, Baik S-H, Ng GYQ, She DT, Balaganapathy P, et al. Evidence that NLRC4 in-
829 flammasome mediates apoptotic and pyroptotic microglial death following ischemic stroke.
830 Brain, Behavior, and Immunity. 2019;75:34–47. https://doi.org/10.1016/j.bbi.2018.09.001

831 20. Cao J, Roth S, Zhang S, Kopczak A, Mami S, Asare Y, et al. DNA-sensing inflammasomes
832 cause recurrent atherosclerotic stroke. Nature. 2024;633:433–41.
833 https://doi.org/10.1038/s41586-024-07803-4

834 21. Bertheloot D, Wanderley CW, Schneider AH, Schiffelers LD, Wuerth JD, Tödtmann JM, et al.
835 Nanobodies dismantle post-pyroptotic ASC specks and counteract inflammation *in vivo*. EMBO
836 Mol Med. 2022;14:e15415. https://doi.org/10.15252/emmm.202115415

837 22. Bellut M, Papp L, Bieber M, Kraft P, Stoll G, Schuhmann MK. NLRP3 inflammasome inhibition
838 alleviates hypoxic endothelial cell death in vitro and protects blood–brain barrier integrity in mu-
839 rine stroke. Cell Death Dis. 2021;13:20. https://doi.org/10.1038/s41419-021-04379-z

840 23. Kleinschnitz C, Stoll G, Bendszus M, Schuh K, Pauer H-U, Burfeind P, et al. Targeting coagula-
841 tion factor XII provides protection from pathological thrombosis in cerebral ischemia without in-
842 terfering with hemostasis. J Exp Med. 2006;203:513–8. https://doi.org/10.1084/jem.20052458

843 24. Kleinschnitz C, De Meyer SF, Schwarz T, Austinat M, Vanhoorelbeke K, Nieswandt B, et al. De-
844 ficiency of von Willebrand factor protects mice from ischemic stroke. Blood. 2009;113:3600–3.
845 https://doi.org/10.1182/blood-2008-09-180695

846 25. Franke M, Bieber M, Stoll G, Schuhmann MK. Validity and Efficacy of Methods to Define
847 Blood Brain Barrier Integrity in Experimental Ischemic Strokes: A Comparison of Albumin West-
848 ern Blot, IgG Western Blot and Albumin Immunofluorescence. MPs. 2021;4:23.
849 https://doi.org/10.3390/mps4010023

850 26. Denes A, Coutts G, Lénárt N, Cruickshank SM, Pelegrin P, Skinner J, et al. AIM2 and NLRC4
851 inflammasomes contribute with ASC to acute brain injury independently of NLRP3. Proc Natl
852 Acad Sci USA. 2015;112:4050–5. https://doi.org/10.1073/pnas.1419090112

853 27. Ray KK, Clarke N, Thornton P, Miles AE, Digby Z, Davies MJ, et al. Anti-Inflammatory Effects of
854 Oral NLRP3 Inhibition With Ruvonoflast Among Individuals at Elevated Cardiovascular Risk.
855 JACC. 2026;88:1981–94. https://doi.org/10.1016/j.jacc.2026.05.014

856 28. Deng Y, Li Z, Sun X, Ma N, Song L, Chen D, et al. TRIM29 (Tripartite Motif Containing 29) Allevi-
857 ates NLRC4 (NLR Family CARD Domain Containing Protein 4) Inflammasome Related Cerebral
858 Injury via Promoting Proteasomal Degradation of NLRC4 in Ischemic Stroke. Stroke.
859 2023;54:1377–89. https://doi.org/10.1161/STROKEAHA.122.038757

860 29. Yang-Wei Fann D, Lee S-Y, Manzanero S, Tang S-C, Gelderblom M, Chunduri P, et al. Intrave-
861 nous immunoglobulin suppresses NLRP1 and NLRP3 inflammasome-mediated neuronal death
862 in ischemic stroke. Cell Death Dis. 2013;4:e790–e790. https://doi.org/10.1038/cddis.2013.326

863 30. Kim H, Seo JS, Lee S-Y, Ha K-T, Choi BT, Shin Y-I, et al. AIM2 inflammasome contributes to
864 brain injury and chronic post-stroke cognitive impairment in mice. Brain, Behavior, and Immun-
865 ity. 2020;S0889159119315156. https://doi.org/10.1016/j.bbi.2020.03.011

866 31. Xue D, Ni F, Liu S, Yan H, Luo Z, Fu G, et al. Atomic mechanisms of full-length ASC-mediated
867 inflammasome assembly. Nat Commun. 2025;16:10564. https://doi.org/10.1038/s41467-025-
868 65578-2

869 32. Bellut M, Strootmann M, Essig F, Stoll G, Vogt ML, Guggenberger K, et al. NLRP3 Marks an In-
870 flammatory Neutrophil–NETosis–Pyroptosis Network in Human Ischemic Stroke Thrombi. Cells.
871 2026;15:1597. https://doi.org/10.3390/cells15171597

872 33. He X, Zeng Y, Li G, Feng Y, Wu C, Liang F, et al. Extracellular ASC exacerbated the recurrent
873 ischemic stroke in an NLRP3-dependent manner. J Cereb Blood Flow Metab.
874 2019;0271678X1985622. https://doi.org/10.1177/0271678X19856226

875 34. Cyr B, Vontell RT, Hadad R, De Rivero Vaccari JP, Keane RW. IC100 blocks inflammasome ac-
876 tivation induced by α-synuclein aggregates and ASC specks. npj Parkinsons Dis. 2025;11:92.
877 https://doi.org/10.1038/s41531-025-00963-8

878 35. De Rivero Vaccari JP, Mim C, Hadad R, Cyr B, Stefansdottir TA, Keane RW. Mechanism of ac-
879 tion of IC 100, a humanized IgG4 monoclonal antibody targeting apoptosis-associated speck-
880 like protein containing a caspase recruitment domain (ASC). Translational Research.
881 2023;251:27–40. https://doi.org/10.1016/j.trsl.2022.06.016

882 36. Lobanova E, Zhang YP, Emin D, Brelstaff J, Kahanawita L, Malpetti M, et al. ASC specks as a
883 single-molecule fluid biomarker of inflammation in neurodegenerative diseases. Nat Commun.
884 2024;15:9690. https://doi.org/10.1038/s41467-024-53547-0

885 37. Li T, Castro-Gomez S, Botella Lucena P, Vieira-Saecker A, Schwartz S, Ding Y, et al. Inflam-
886 masome adaptor ASC promotes sustained neuroinflammation and mild cognitive impairment in
887 a closed-head injury model. Journal of Clinical Investigation [Internet]. 2026 [cited 2026 Mar 10];
888 https://doi.org/10.1172/JCI199818

889

Supplementary Files

This is a list of supplementary files associated with this preprint. Click to download.

- AdditionalFile1.docx
- AdditionalFile2.docx